

1 **Classification:** Biological Sciences – Applied Biological Sciences; Physical Sciences -
2 Engineering
3
4

5 **Title:** Development of an autonomous and bifunctional quorum-sensing circuit for metabolic
6 flux control in engineered *Escherichia coli*
7
8

9 **Authors:** Christina V. Dinh and Kristala L. J. Prather
10
11

12 **Author affiliation:** Department of Chemical Engineering, Massachusetts Institute of
13 Technology, Cambridge, MA 02139
14
15

16 **Author emails:** cdinh@mit.edu, kljp@mit.edu
17
18

19 **Corresponding author:** Kristala L. J. Prather
20
21

22 **Keywords:** Synthetic biology, metabolic engineering, dynamic control
23
24
25
26
27
28
29
30

31 **Abstract**

32
33 Metabolic engineering seeks to reprogram microbial cells to efficiently and sustainably produce
34 value-added compounds. Since chemical production can be at odds with the cell's natural
35 objectives, strategies have been developed to balance conflicting goals. For example, dynamic
36 regulation modulates gene expression to favor biomass and metabolite accumulation at low cell-
37 densities before diverting key metabolic fluxes towards product formation. To trigger changes in
38 gene expression in a pathway-independent manner without the need for exogenous inducers,
39 researchers have coupled gene expression to quorum-sensing (QS) circuits, which regulate
40 transcription based on cell-density. While effective, studies thus far have been limited to one
41 control point. More challenging pathways may require layered dynamic regulation strategies,
42 motivating the development of a generalizable tool for regulating multiple sets of genes. We
43 have developed a QS-based regulation tool that combines components of the *lux* and *esa* QS
44 systems to simultaneously and dynamically up- and down-regulate expression of two sets of
45 genes. Characterization of the circuit revealed that varying the expression level of two QS
46 components leads to predictable changes in switching dynamics and that using components from
47 two QS systems allows for independent tuning capability. We applied the regulation tool to
48 successfully address challenges in both the naringenin and salicylic acid synthesis pathways.
49 Through these case studies, we confirmed the benefit of having multiple control points,
50 predictable tuning capabilities, and independently tunable regulation modules.

51

52

53 **Significance statement**

54

55 Efficient microbial synthesis in challenging pathways relies on dynamic regulation of multiple
56 metabolic fluxes to balance several competing goals. To address these situations, we developed
57 an autonomous, pathway-independent, and layered regulation tool. By incorporating parts from
58 two different QS systems, the layers of our system can be tuned independently to ensure
59 generalizability. Application of the regulation system to overcoming two different sets of
60 challenges in the naringenin and salicylic acid pathways resulted in significant improvements in
61 titer, demonstrating that the system is an effective tool for improving pathway production.

62

63

64

65 **Introduction**

66

67 Metabolic engineering seeks to reprogram cells with the goal of producing value-added
68 chemicals that are well suited to microbial synthesis. Such chemicals vary widely, including ones
69 used in biofuels, plastics, and pharmaceuticals. Enzymes that produce stereochemically pure
70 products simplify downstream separation requirements in fine chemical production. For
71 commodity chemical production, microbial synthesis may allow for utilization of inexpensive or
72 renewable feedstocks. Additionally, microbial synthesis typically occurs under mild conditions,
73 offering safety, energy conservation, and environmental benefits.

74

75 Challenges that limit efficient production can arise when heterologous pathways are imported
76 into host organisms. For example, flux through heterologous pathways may inhibit cell growth
77 by generating toxic products or consuming essential endogenous metabolites. Strategies for
78 overcoming these challenges focus on balancing growth and production through controlling
79 reaction fluxes. The static balancing approach aims to maintain fixed reaction fluxes in an
80 intermediate regime such that neither objective dominates whereas the dynamic approach
81 generally regulates gene expression to favor accumulating biomass or key metabolites early,
82 before diverting metabolic fluxes towards product formation. While more difficult to implement
83 in practice, dynamic control is required for efficient production in some pathways.

84

85 Successful dynamic flux regulation strategies have been experimentally demonstrated in a
86 number of production pathways by controlling activity of key pathway enzymes at the
87 transcriptional or post-translational level. Many recent studies have focused on self-actuating
88 dynamic control methods to minimize required human supervision and to avoid use of
89 exogenous inducers, which can be costly. These control systems couple expression of pathway
90 genes, anti-sense RNA, CRISPRi components, or proteases to relevant conditions such as
91 external signals (1), internal cell state (metabolites, growth state, stress state) (2–10), cell-density
92 (11–13), glucose concentration (14, 15), or a combination of these (16–18). Control systems
93 which respond to pathway-independent signals such as cell-density or O₂ level offer the
94 additional advantage of applicability across different synthesis pathways without development of
95 a new sensor for the relevant metabolite in each pathway. However, to our knowledge, there has
96 not yet been a fully pathway-independent dynamic control system for independently regulating
97 multiple metabolic fluxes, which may be required for efficient production of more challenging
98 pathways.

99

100 With the goal of developing such a control system, we constructed a circuit containing genetic
101 components from the *lux* and *esaR* QS systems. This system contains two constitutively
102 expressed genes for the regulator proteins, LuxR and EsaR, which activate and repress the P_{lux}
103 and P_{esaR} promoters, respectively, upon binding. The binding affinity between the regulators and
104 their cognate promoters depends on the level of a common signaling molecule, 3-oxohexanoyl

105 homoserine lactone (AHL) and thus, we can dynamically regulate the transcription level of the
106 promoters in a cell-density dependent manner by constitutively expressing the gene encoding the
107 AHL synthase, *esaI*. To ensure this system can be used to explore a broad metabolic control
108 space, we varied the *luxR* and *esaI* expression levels to obtain a range of switching dynamics.
109 The engineered regulatory circuits were applied towards controlling metabolic fluxes in two
110 different synthesis pathways with unique trade-offs and metabolic control points. The significant
111 improvement in product titers upon implementation of the control system in both case studies
112 demonstrates the effectiveness of the control circuit for balancing multiple design objectives in
113 synthesis pathways.

114

115

116 **Results**

117

118 *Characterization of QS-based autonomous induction*

119

120 We characterized two QS circuits for autonomous and dynamic gene expression control. The
121 first QS circuit uses the transcriptional regulator LuxR, which forms a complex with AHL to
122 activate transcription from the P_{lux} promoter (Figure 1A, left). For the second QS circuit, we
123 constructed a hybrid promoter (P_{esaR-H}) that contains an EsaR binding site (*esaO*) downstream of
124 the transcription start site of the P_{trc} promoter. In the absence of AHL, EsaR binds to the *esaO*
125 sequence, repressing transcription from P_{esaR-H} . Upon binding to AHL, EsaR can no longer bind
126 to the operator sequence, leading to de-repression (Figure 1A, right). Each circuit can be used to
127 dynamically upregulate the expression of any gene of interest by placing the gene downstream of
128 the P_{lux} or P_{esaR-H} promoters.

129

130 Gupta et al. showed that the rate of AHL accumulation can be controlled by varying the
131 constitutive expression level of the gene for the AHL synthase, *esaI* (13). By changing the AHL
132 accumulation rate, we can tune the switching dynamics of these circuits. When applied to
133 regulating enzyme expression, this tunability corresponds with the ability to vary the schedule of
134 metabolic flux regulation in search for one that suits the desired application. To characterize
135 relative switching dynamics from the P_{lux} and P_{esaR-H} promoters, *esaI* was integrated into
136 BL21(DE3) under a library of promoter and RBS variants to make the BL21-LXX strain series.
137 A P_{lux} or P_{esaR-H} promoter driving *mCherry* expression on a medium-copy plasmid (pCOLA- P_{lux} -
138 *mCherry* or pCOLA- P_{esaR-H} -*mCherry*) was introduced into the BL21-LXX strain series. Strains
139 testing the P_{lux} promoter required an additional plasmid with the *luxR* gene constitutively
140 expressed from an Anderson library promoter (BBa_J23114) and varying RBS's on a low-copy
141 plasmid (pACYC- P_{con} -RBSX-*luxR*). The pCOLA- P_{esaR-H} -*mCherry* vector contains *esaR*
142 constitutively expressed from a BIOFAB library promoter (apFAB104).

143

144 Continuous fluorescence measurements of these strains produced a range of switching times in
145 the up-regulation mode. In general, increasing the *esaI* expression level leads to earlier switching
146 with both promoters (Figure 1B) and increasing the *luxR* expression level results in earlier
147 switching from the P_{lux} promoter only (Figure 1C). These trends are consistent with expectations
148 based on our understanding of the interactions in the QS circuits (Figure 1D).

149

150

151 *Dynamic gene regulation to control flux through the naringenin pathway*

152

153 Naringenin is a natural plant-produced compound that is a common precursor of most
154 flavonoids, natural plant products with a number of desirable therapeutic characteristics
155 including anti-cancer and antiviral activity (19–21). One naringenin production pathway uses
156 four enzymatic reactions to convert L-tyrosine and malonyl-CoA to (2S)-naringenin (Figure 2A).
157 This pathway has been widely studied in *E. coli* as a model system with relatively well-
158 characterized challenges that may be addressed through dynamic control (22–26). For this
159 reason, we applied our regulation system towards alleviating the limitations of the naringenin
160 pathway.

161

162 Results from previous studies suggest that efficient naringenin production relies on maintaining
163 high levels of chalcone synthase (CHS) and chalcone isomerase (CHI) relative to tyrosine
164 ammonia lyase (TAL) and 4-coumaryl-CoA lyase (4CL), possibly due to an inhibitory
165 interaction of coumaryl-CoA against TAL (22). This balance can be reached by delaying
166 expression of *TAL* and *4CL*, while constitutively expressing *CHS* and *CHI* (22). To confirm that
167 QS-based regulation can achieve this balancing effect, *TAL* and *4CL* were expressed from P_{lux} or
168 P_{esaR-H} promoters (pCOLA- P_{lux} -*TAL*- *4CL* or pCOLA- P_{esaR-H} -*TAL*- *4CL*) while *CHI* and *CHS*
169 were each expressed from T7 promoters (pET-*CHI-CHS*), with IPTG added at inoculation. These
170 plasmids, along with one that constitutively expresses *luxR* (pACYC- P_{con} -RBSX-*luxR*), were
171 transformed into the BL21-LXX strain series to produce a set of strains that dynamically up-
172 regulate *TAL* and *4CL* expression at varying cell densities.

173

174 Comparison of naringenin titers from dynamically and statically controlled strains confirmed that
175 the naringenin pathway benefits from dynamic regulation of *TAL* and *4CL* expression under both
176 the P_{lux} and P_{esaR-H} promoters (Figure 2B-C). With *TAL* and *4CL* expression under the P_{lux}
177 promoter, static expression strains (i.e., with exogenous AHL added at inoculation) produced less
178 than 10 μ M naringenin, significantly less than the $204 \pm 5 \mu$ M naringenin produced from the top
179 strain with autonomous dynamic *TAL* and *4CL* regulation. Similarly, static *TAL* and *4CL*
180 expression controlled from P_{esaR-H} promoters produced less than 30 μ M naringenin, also
181 significantly less than the $196 \pm 2 \mu$ M produced from the top autonomous dynamic strain. In
182 both the P_{lux} - and P_{esaR-H} -controlled systems, an intermediate *esaI* expression level resulted in the
183 maximum naringenin titer. This trend agrees with our current understanding of the pathway as

184 early-switching strains might be subject to TAL inhibition and late-switching strains might be
185 limited by low pathway fluxes. At the intermediate *esaI* level, naringenin titers from both QS
186 circuits matched or exceeded those obtained with exogenous AHL addition, suggesting that the
187 autonomous switching strategy can successfully replace exogenous inducer addition in this
188 context.

189

190 Previous studies have suggested that naringenin production in *E. coli* is additionally limited by
191 low endogenous malonyl-CoA levels (22, 25, 26). To confirm that this limitation exists in our
192 system, all strains were cultured with and without cerulenin, an inhibitor of fatty acid synthesis
193 that is known to elevate malonyl-CoA levels (27). Naringenin titers improved in all strains when
194 cultured with cerulenin as expected, confirming that malonyl-CoA pools are limiting (Figure 2B
195 and Figure 2C). In an effort to improve the naringenin titers using the P_{lux} -control system to
196 match the top titer using the P_{esaR} -control system, we explored additional P_{lux} switching
197 dynamics by testing additional *esaI* and *luxR* expression levels. However, none resulted in
198 improved naringenin titers (Figures S1 and S2) and therefore, we decided to further build upon
199 the regulation scheme with the P_{esaR-H} promoter controlling *TAL* and *4CL* expression.

200

201

202 *Dynamic down-regulation of endogenous gene expression for malonyl-CoA accumulation*
203 *improves naringenin titers*

204

205 While effective, cerulenin is not a cost-efficient solution for increasing malonyl-CoA pools and
206 thus, we aimed to dynamically silence gene expression by using the P_{lux} promoter to drive
207 expression of *dCas9* and guide RNA(s) (*sgRNA*) targeted towards dynamically down-regulating
208 the gene(s) of interest. To characterize the down-regulation behavior, two P_{lux} promoters driving
209 *dCas9* and *sgGFP* expression on low- and medium-copy plasmids, respectively (pACYC- P_{lux} -
210 *dCas9*- $P_{con10-luxR}$ and pCDF- P_{lux} -*sgGFP*), were introduced into the BL21-LXX strain series
211 along with a plasmid that expresses degradation-tagged GFP (pTrc-*GFP-LVA*) (Figure S3A). In
212 general, silencing dynamics from the P_{lux} promoter follow the expected trends based on the
213 previous characterization of the *lux* circuit. That is, increasing *esaI* or *luxR* expression level leads
214 to earlier *dCas9* and *sgRNA* expression and earlier down-regulation of the GFP signal (Figure
215 S3B-C).

216

217 *dCas9* and *sgRNAs* targeted towards endogenous genes were expressed from the P_{lux} promoter
218 (Figure 3C), with combinations of target genes chosen based on results from a previous study
219 that used CRISPRi to elevate malonyl-CoA pools by down-regulating competing acetyl-CoA-
220 consuming reactions and fatty acid synthesis cycle reactions (Figure S4) (26). The P_{lux} -*sgRNA*
221 expression cassettes were expressed from the pCDF vector backbone and the P_{lux} -*dCas9* cassette
222 and P_{con} -*luxR* variants were expressed from pACYC. To ensure that the down-regulation module
223 was having the desired effects, we first confirmed that transcript levels of the target gene are
224 down-regulated in an *EsaI* level-dependent manner (Figure S5). We additionally confirmed that

225 the decreased transcript levels resulted in elevated malonyl-CoA levels by utilizing a previously
226 developed fluorescence-based sensor (8) (Figure S6).

227
228 The plasmids harboring the P_{lux} down-regulation module (Figure 3C) were then imported into the
229 naringenin producing strains which control *TAL* and *4CL* expression under the P_{esaR-H} promoter
230 (Figure 3B). Based on the previous observation that the L19-*esaI* expression level resulted in the
231 highest naringenin titers under all conditions, we combinatorically tested LuxR levels and *sgRNA*
232 target genes in the BL21-L19 strain background. Under this dual-regulation scheme (Figure 3A-
233 C), increasing cell density leads to dynamic down-regulation of the *sgRNA* target genes and
234 dynamic up-regulation of coumaryl-CoA-producing reactions. The library of LuxR levels and
235 *sgRNA* targets resulted in a set of strains that produced varying naringenin titers (Figure 3E and
236 Figure S7). Every strain with dual-regulation resulted in higher naringenin titers compared to the
237 non-specific *sgRNA* control and half of the library resulted in higher naringenin titers compared
238 to the cerulenin-treated non-specific *sgRNA* control, suggesting that the down-regulation module
239 can effectively replace cerulenin addition in this context (Figure 3D and Figure S7). The top
240 producer identified through this screen yields $463 \pm 1 \mu\text{M}$ naringenin, 140% higher than the
241 strain with only the up-regulation module and 40% higher than the cerulenin-treated strain.
242 Fermentation of the top producer at a bench-top bioreactor scale confirms that the improvement
243 achieved through dual-regulation holds across fermentation scales (Figure S8).

244
245
246 *Dual-regulation for salicylic acid production*
247
248 To test the generalizability of the regulatory circuits, we sought to apply the regulation strategy
249 to a different production pathway that might also benefit from two points of dynamic control.
250 One such pathway is the salicylic acid production pathway, which converts endogenous
251 chorismate to salicylic acid using the enzymes, isochorismate synthase (*Ics*) and isochorismate
252 pyruvate lyase (*Ipl*), produced from the genes *entC* and *pchB*, respectively (Figure 4A). Since
253 salicylic acid can burden growth of *E. coli*, we hypothesized that production could be improved
254 by delaying expression of pathway genes to manage the trade-off between growth and
255 production. Additionally, chorismate is naturally consumed by the cell to produce the aromatic
256 amino acids such that knocking out the consumption reactions to divert chorismate towards
257 salicylic acid production results in an auxotrophic strain that requires aromatic amino acid
258 supplementation. To create a salicylic acid producer that does not rely on amino acid
259 supplementation, we used the dual-regulation system to (1) dynamically up-regulate *entC* and
260 *pchB* expression to alleviate the growth burden and (2) dynamically down-regulate *pheA* and
261 *tyrA* expression to divert chorismate pools towards the salicylic acid production pathway without
262 introducing auxotrophies.

263
264 To implement the proposed control strategy, *entC* and *pchB* were expressed under the P_{esaR-H}
265 promoter and *dCas9* and *sgRNAs* targeted towards *pheA* and *tyrA* were expressed from the P_{lux}

266 promoter. The P_{esaR-H} -*entC*, P_{esaR-H} -*pchB*, and P_{con} -*esaR* cassettes were expressed from the
267 pCOLA-duet backbone (pCOLA- P_{esaR-H} -*entC*-*pchB*, Figure 4B). *dCas9* was expressed from the
268 same plasmids as in the naringenin experiments (pACYC- P_{lux} -*dCas9*- P_{con} -RBSX-*luxR*) and the
269 P_{lux} -*sgRNA* cassette was expressed from the pCDF backbone (pCDF- P_{lux} -*sg-pheA-tyrA*, Figure
270 4C). We tested this set of plasmids in a phenylalanine producer strain background that is
271 commonly used for salicylic acid production (NST74) (28), with genetically integrated *esaI*
272 (NST74-LXX). Under the proposed regulatory scheme, we can tune the up- and down-regulation
273 modules by varying *EsaI* level and can tune the down-regulation module only by varying the
274 LuxR level. Rather than holding expression of one of the QS components (*EsaI* or LuxR)
275 constant in the optimization, we decided to combinatorially vary both since we were only
276 interested in one combination of down-regulation targets in this context.

277
278 Dynamically controlling *entC* and *pchB* expression only and testing salicylic acid production
279 over a range of *esaI* expression levels resulted in a maximum observed salicylic acid titer of 291
280 \pm 3 mg/L, a 10% improvement over that static strain with *entC* and *pchB* induced at inoculation.
281 Addition of the down-regulation module and exploration of *EsaI* and LuxR levels resulted in a
282 strain that produced 520 \pm 7 mg/L salicylic acid, a 1.8-fold improvement over the static strain
283 (Figure 4D and Figure S9). This application demonstrates the generalizability of our control
284 tool, confirming that independent control of two different targets—or sets of targets—can
285 significantly improve production in some pathways.

286
287

288 **Conclusions**

289

290 Dynamic regulation is an important strategy in metabolic engineering for improving production
291 in challenging pathways. We have developed an autonomous, pathway-independent, tunable, and
292 bifunctional gene expression regulation system that can be applied to metabolic flux control. The
293 system was applied to controlling key heterologous and endogenous enzymes in the naringenin
294 and salicylic acid pathways, resulting in production benefits in both case studies. Our work
295 demonstrates the importance of having two independently tunable modes of control for dynamic
296 regulation to effectively manage trade-offs and builds on the collection of tools available for
297 developing industrially feasible microbial production strains.

298
299

300 **Materials and Methods**

301

302 All strains and plasmids used in this study are summarized in Tables S1 and S2, respectively.
303 Sequences for promoters and RBS sequences are provided in Table S3; the codon optimized
304 sequences for *TAL*, *4CL*, *CHS*, and *CHI* are provided in Supplemental Table 4; and guide RNA
305 sequences are provided in Supplemental Table 5. For plasmid construction and gene/genome

306 editing, cells were cultured in Luria-Bertani (LB) broth at either 30 °C or 37 °C. Temperature-
307 sensitive plasmids were cured at 42 °C.

308

309

310 Strain construction

311

312 *Synthase expression library integrations.* The *esaI* expression cassette was integrated into the
313 genome under the control of several different constitutive synthetic promoters (denoted BL2-
314 LXX or NST74-LXX) (13). Integration was performed via “clonetegration” (29). The desired
315 *Esal* expression cassette was inserted into the pOSIP-KO backbone using restriction digestion
316 and ligation. The ligation product was used to transform *E. coli* strain BL21(DE3) or NST74 for
317 integration into the 186 locus. The phage integration genes and antibiotic resistance cassette were
318 cured by transforming with a plasmid containing FLP under control of the P_{tet} promoter (pTet-
319 FLP), yielding strains BL21-LXX or NST-LXX.

320

321 *Fluorescence characterization of QS circuits.* The P_{lux} promoter was amplified from pSB1A2-
322 P_{lux} -*GFP*(30) using primers CD_211 and CD_212, *mCherry* was amplified from pFM301 (p15A
323 ori, kanamycin resistance, *mCherry*-BBa_J06504 under constitutive promoter BBa_J23101)
324 using primers CD_213 and CD_214, and the two products were joined using splicing by overlap
325 extension PCR to yield P_{lux} -*mCherry*. This cassette was inserted into a modified pCOLA
326 backbone without the T7 system components using restriction digestion and ligation to yield
327 pCOLA- P_{lux} -*mCherry*. The P_{con10} -*luxR* cassette was amplified from pSB1A2- P_{lux} -*GFP*- P_{con10} -
328 *luxR* (30) using primers CD_215 and CD_216 and inserted into the pACYC backbone using
329 restriction digestion and ligation to yield pACYC- P_{con10} -*luxR*. The strength of the RBS driving
330 *luxR* was decreased using primers lux_R1_a and luxR_R1_b and increased using primers
331 luxR_R3_a, luxR_R3_b, luxR_R4_a, and luxR_R4_b, through Golden Gate cloning.

332

333 The P_{trc} promoter was amplified from the pTrc99A vector with the *esaO* operator sequence in
334 place of the *lacO* sequence to yield the P_{trc} -*esaO* fragment (P_{esaR-H}) using primers esa_RFP_5 and
335 esa_RFP_6. *mCherry* was amplified from pFM301 using esa_RFP_7 and esa_RFP8, *esaR* from a
336 constitutive BIOFAB library promoter was amplified from pSB3K3- P_{esaR} -*GFP*- P_{con} -*esaR*(31)
337 using esa_RFP_3 and esa_RFP_4, and the pCOLA backbone was amplified using esa_RFP_1
338 and esa_RFP_2. These PCR products were assembled into the vector pCOLA- P_{esaRH} -*mCherry*
339 using Golden Gate cloning.

340

341 A custom synthesized gene fragment which contains BsaI restriction sites followed by the
342 *sgRNA* scaffold sequence, flanked on both sides with bidirectional terminator B0015 (Genscript,
343 New Jersey, USA), was amplified using primers sg_3 and sg_10. The pCDF backbone was
344 amplified using primer sg_1 and sg_2. These two PCR products were combined to make pCDF-
345 BsaI-BsaI-*sgRNA* using Golden Gate cloning. The 20-bp guide sequence targeting GFPmut3b

346 was appended to P_{lux} using overhang PCR using the template pSB1A2- P_{lux} -*GFP* and primers
347 A11 and A12 and inserted into pCDF-BsaI-BsaI-*sgRNA* using Golden Gate cloning to yield
348 pCDF- P_{lux} -*sgGFP*.

349
350 *dCas9* was amplified from pdCas9(32) with SapI sites preceding the gene using primers C9_1
351 and C9_2 and inserted into the pACYC backbone using restriction digestion and ligation to yield
352 pACYC-SapI-SapI-*dCas9*. The P_{lux} promoter was PCR amplified from pSB1A2- P_{lux} -*GFP* (30)
353 using primers A15 and A16, which add flanking SapI sites, and inserted into pACYC-SapI-SapI-
354 *dCas9* using Golden Gate cloning to yield pACYC- P_{lux} -*dCas9*. The RBS variants of the *luxR*
355 cassette were amplified using C9_lux_3 and C9_lux_4 and the pACYC- P_{lux} -*dCas9* plasmid was
356 amplified using C9_lux_1 and C9_lux_2. The resulting products were assembled using Golden
357 Gate cloning to yield pACYC- P_{lux} -*dCas9*- P_{con} -RBSX-*luxR*.

358
359 *Malonyl-CoA biosensor*. The *lacI*- P_{T7} -*fapR* cassette was amplified from the pCDM4-*fapR*
360 plasmid using primers fapR_3 and fapR_4 and the pCOLA backbone was amplified using
361 fapR_1 and fapR_2⁸. The two products were assembled using Golden Gate cloning to yield
362 pCOLA-*fapR*. This modification was to maintain origin of replication compatibility only.

363
364 *Naringenin pathway*. For QS-based transcriptional control of *TAL* and *4CL*, codon optimized
365 sequences of each gene appended to P_{lux} were inserted into pCOLA using restriction digestion
366 and ligation to yield pCOLA- P_{lux} -*TAL*-*4CL*_v1 (Genscript, New Jersey, USA). The final
367 pCOLA- P_{lux} -*TAL*-*4CL* plasmid used in this study was obtained using primers T4_R20_(1-8)
368 using Golden Gate cloning. This modification was carried out to take out the T7 system
369 components from the backbone and to increase the strength of the RBS's driving *TAL* and *4CL*
370 expression. Codon optimized sequences of *CHS* and *CHI* (Genscript, New Jersey, USA) were
371 PCR amplified using primers CHS_T7F2 and CHS_T7R2 for *CHS* and CHI_T7F2 and
372 CHI_T7R2 for *CHI*. Products were digested and ligated into MCS1 and MCS2 of the pET-duet
373 vector to yield pET-*CHS*-*CHI*.

374
375 *Dynamic control of ICS and IPL in the salicylic acid pathway*. For QS-based transcriptional
376 control of the genes encoding isochorismate synthase (*Ics*) and isochorismate pyruvate lyase
377 (*Ipl*), the pCOLA backbone was amplified using EP_1 and EP_2, *esaR* was amplified from
378 pSB3K3- P_{esaR} -GFP-p104-*esaR* using EP_3 and EP_4, P_{esaR-H} was amplified from pCOLA- P_{esaR} -
379 H-mCherry using EP_5 and EP_6 along with EP_9 and EP_10, *entC* (encoding *Ics*) was
380 amplified from the *E. coli* genome using EP_7 and EP_8, and *pchB* (encoding *Ipl*) was amplified
381 from the *Pseudomonas aeruginosa* genome using EP_11 and EP_12. The PCR products were
382 assembled into the vector pCOLA- P_{esaR-H} -*entC*-*pchB* using Golden Gate cloning.

383
384 *CRISPRi-mediated control of endogenous enzymes*. For QS-based silencing of endogenous
385 genes, the 20-bp guide sequence was changed from pCDF- P_{lux} -*sgGFP* by circular polymerase

386 extension cloning using primers [gene name]_luxR_F, [gene name]_luxR_R, sg_CPEC_1 and
387 sg_CPEC_2. The 20-bp guide sequences were obtained from either previous studies(26) or using
388 predictions from ATUM's sgRNA design tool (www.atum.bio). To produce vectors which
389 express multiple guides under the control of individual promoters, the pCDF-P_{lux}-sgRNA vectors
390 which express a single guide RNA were used as templates in Golden Gate cloning using primer
391 sg_(1-10).

392

393 **Culturing and fermentations**

394

395 *Fluorescence characterization.* Switching dynamics over varying expression levels of QS circuit
396 components (*esaI* and *luxR*) were quantified using the BioLector microbioreactor system (m2p-
397 labs, Baesweiler, Germany). Individual colonies were inoculated in LB medium and grown
398 overnight at 30 °C. 1 mL cultures were inoculated from these seeds at OD₆₀₀ 0.05 into BioLector
399 48-well flower plates and incubated at 30 °C, 1200 rpm (3 mm orbit), and 80% relative humidity.
400 The plate was sealed with a gas-permeable sealing foil (m2p-labs). Cultures were monitored for
401 OD (BioLector units), GFP, and RFP fluorescence over time.

402

403 *Fermentations.* Naringenin production trials were performed in glass vials with 5 mL working
404 volume at 30 °C and 80% humidity with 250 rpm shaking in modified MOPS minimal medium
405 containing 5 g/L D-glucose, 500 mg/L tyrosine, 4 g/L NH₄Cl, 1 g/L K₂HPO₄, 2 mM MgSO₄, 0.1
406 mM CaCl₂, 40 mM MOPS, 4 mM Tricine, 50 mM NaCl, 100 mM Bis-Tris, 143 uM EDTA, 31
407 uM FeCl₃, 6.2 uM ZnCl₃, 0.76 uM CuCl₂, 0.42 uM CoCl₂, 1.62 uM H₃BO₃ and 0.081 uM
408 MnCl₂. For strains containing plasmids with pET, pCOLA, pACYC, and pCDF vector
409 backbones, the medium was also supplemented with 100 µg/mL carbenicillin, 50 µg/mL
410 kanamycin, 34 µg/mL chloramphenicol, and 100 µg/mL spectinomycin, respectively, for
411 plasmid maintenance. Strains were initially grown in 3 mL of LB medium at 30 °C overnight,
412 then diluted 1:100 into 3-mL seed cultures of modified MOPS medium for ~24 h at 30 °C. These
413 were used to inoculate working cultures at OD₆₀₀ 0.05. Samples were taken periodically for
414 quantification of cell density and extracellular metabolites. Fermentations were carried out for 48
415 hours.

416

417 For naringenin bioreactor production trials, colonies were inoculated into 50-mL seed cultures in
418 250-mL baffled shake flasks and incubated at 30 °C, 250 rpm, 8% humidity for ~16 h. Seed
419 cultures were then used to inoculate a 3-L Labfors bioreactor (Infors AG, Bottmingen,
420 Switzerland; 1 L working volume) at OD₆₀₀ 0.05. The pH was controlled at 7 using 4 M NaOH.
421 DO was controlled at 35% of maximum saturation by agitation rate (250-1000 rpm) and constant
422 air sparging at 1 L per minute. Batch fermentation was carried out for 48 h, with 5-mL samples
423 removed at 18, 24, and 48 h for optical density and titer measurements.

424

425 Salicylic acid production trials were performed in BioLector 48-well flower plates (m2p-labs,
426 Baesweiler, Germany) with 1 mL working volume and 37 °C and 80% humidity with 900 rpm
427 shaking in M9 minimal medium containing 10 g glycerol, 2.5 g glucose, 6g Na₂HPO₄, 0.5 g
428 NaCl, 3 g KH₂PO₄, 1 g NH₄Cl, 245 mg MgSO₄·7H₂O, 14.7 mg CaCl₂·2H₂O, 2 g MOPS, and
429 micronutrients including 2.0 mg vitamin B1, 1.25 mg H₃BO₃, 0.15 mg NaMoO₄·2H₂O, 0.7 mg
430 CoCl₂·2H₂O, 0.25 mg CuSO₄·5H₂O, 1.6 mg MnCl₂·4H₂O, and 0.3 mg ZnSO₄·7H₂O per liter. For
431 strains containing plasmids with pCOLA, pACYC, and pCDF vector backbones, the medium
432 was supplemented with 50 µg/mL kanamycin, 34 µg/mL chloramphenicol, and 100 µg/mL
433 spectinomycin, respectively, for plasmid maintenance. Strains were initially grown in 1 mL of
434 M9 medium at 37 °C overnight and these cultures were used to inoculate working cultures at
435 OD₆₀₀ 0.05. Samples were taken periodically for quantification of cell density and extracellular
436 metabolites. Fermentations were carried out for 24 hours.

437

438

439 **Quantification of metabolites**

440

441 Tyrosine, *p*-coumaric acid, naringenin, and salicylic acid were quantified by high performance
442 liquid chromatography (HPLC) on an Agilent 1100 series instrument (Santa Clara, CA) with a
443 ZORBAX Eclipse column (4.6 mm x 150 m x 3.5 um). The HPLC was run with a mixture of
444 solution A (water + 0.1% TFA) and solution B (acetonitrile + 0.1% TFA) as the eluent at a flow
445 rate of 1 mL/min. The following gradient was used: at 0 min, 90% solution A and 10% solution
446 B, by 10 mins, 60% solution A and 40% solution B, by 15 mins, 40% solution A and 60%
447 solution B, by 15.5 mins, 0 % solution A and 100% solution B, 15.5 – 21 min, 0 % solution A
448 and 100 % solution B, by 21.5 min, 90% solution A and 10% solution B, 21.5 – 28 min, 90%
449 solution A and 10% solution B. Compounds were quantified with 10 µL injections using diode-
450 array detection at 270 nm (tyrosine) or 290 nm (*p*-coumaric acid, naringenin, and salicylic acid).

451

452

453 **Statistics**

454

455 All error bars are reported as standard deviations of replicates. The number of replicates is
456 provided in the corresponding figure caption.

457

458

459 **Data availability**

460

461 All data generated and analyzed and analyzed in this study are available from the corresponding
462 author upon reasonable request.

463

464

465 **Acknowledgements**

466
467 We thank the C. Voigt lab (MIT, Biological Engineering) for kindly providing the plasmid
468 pFM301 and the M. Koffas lab (Rensselaer Polytechnic Institute, Chemical and Biological
469 Engineering) for kindly providing the malonyl-CoA sensor plasmids. This work was supported
470 by the US National Science Foundation through the Division of Molecular and Cellular
471 Biosciences (Grant No. MCB-1517913 and MCB-1817708).

472

473

474 **References**

475

- 476 1. E. Nevoigt, *et al.*, Engineering Promoter Regulation. *Biotechnol. Bioeng.* **96**, 550–558
477 (2006).
- 478 2. W. R. Farmer, J. C. Liao, Improving lycopene production in *Escherichia coli* by
479 engineering metabolic control. *Nat. Biotechnol.* **18**, 533–537 (2000).
- 480 3. Z. Kang, Q. Wang, H. Zhang, Q. Qi, Construction of a stress-induced system in
481 *Escherichia coli* for efficient polyhydroxyalkanoates production. *Appl. Microbiol.*
482 *Biotechnol.* **79**, 203–208 (2008).
- 483 4. Q. Liang, H. Zhang, S. Li, Q. Qi, Construction of stress-induced metabolic pathway from
484 glucose to 1,3-propanediol in *Escherichia coli*. *Appl. Microbiol. Biotechnol.* **89**, 57–62
485 (2011).
- 486 5. F. Zhang, J. M. Carothers, J. D. Keasling, Design of a dynamic sensor-regulator system
487 for production of chemicals and fuels derived from fatty acids. *Nat. Biotechnol.* **30**, 354–
488 359 (2012).
- 489 6. R. H. Dahl, *et al.*, Engineering dynamic pathway regulation using stress-response
490 promoters. *Nat. Biotechnol.* **31**, 1039–1046 (2013).
- 491 7. S. Siedler, S. G. Stahlhut, S. Malla, J. Maury, A. R. Neves, Novel biosensors based on fl
492 avonoid-responsive transcriptional regulators introduced into *Escherichia coli*. *Metab.*
493 *Eng.* **21**, 2–8 (2014).
- 494 8. P. Xu, L. Li, F. Zhang, G. Stephanopoulos, M. Koffas, Improving fatty acids production
495 by engineering dynamic pathway regulation and metabolic control. *Proc. Natl. Acad. Sci.*
496 **111**, 11299–11304 (2014).
- 497 9. S. J. Doong, A. Gupta, K. L. J. Prather, Layered dynamic regulation for improving
498 metabolic pathway productivity in *Escherichia coli*. *Proc. Natl. Acad. Sci.* **115**, 2964–
499 2969 (2018).
- 500 10. Y. Yang, *et al.*, Sensor-regulator and RNAi based bifunctional dynamic control network
501 for engineered microbial synthesis. *Nat. Commun.* **9**, 1–10 (2018).
- 502 11. Y. Soma, T. Hanai, Self-induced metabolic state switching by a tunable cell density sensor
503 for microbial isopropanol production. *Metab. Eng.* **30**, 7–15 (2015).
- 504 12. H. Liu, T. Lu, Autonomous production of 1,4-butanediol via a de novo biosynthesis
505 pathway in engineered *Escherichia coli*. *Metab. Eng.* **29**, 135–141 (2015).
- 506 13. A. Gupta, I. M. B. Reizman, C. R. Reisch, K. L. J. Prather, Dynamic regulation of
507 metabolic flux in engineered bacteria using a pathway-independent quorum-sensing
508 circuit. *Nat. Biotechnol.* **3** (2017).
- 509 14. W. Xie, L. Ye, X. Lv, H. Xu, H. Yu, Sequential control of biosynthetic pathways for

balanced utilization of metabolic intermediates in *Saccharomyces cerevisiae*. *Metab. Eng.* **28**, 8–18 (2015).

15. W. Bothfeld, G. Kapov, K. E. J. Tyo, A Glucose-Sensing Toggle Switch for Autonomous, High Productivity Genetic Control. *ACS Synth. Biol.* **6**, 1296–1304 (2017).

16. T. M. Lo, S. H. Chng, W. S. Teo, H. S. Cho, M. W. Chang, A Two-Layer Gene Circuit for Decoupling Cell Growth from Metabolite Production. *Cell Syst.* **3**, 133–143 (2016).

17. X. He, Y. Chen, Q. Liang, Q. Qi, Autoinduced AND Gate Controls Metabolic Pathway Dynamically in Response to Microbial Communities and Cell Physiological State. *ACS Synth. Biol.* **6**, 463–470 (2017).

18. F. Moser, *et al.*, Dynamic control of endogenous metabolism with combinatorial logic circuits. *Mol Syst Biol* **14**, 8605 (2018).

19. Z. L. Fowler, M. A. G. Koffas, Biosynthesis and biotechnological production of flavanones: Current state and perspectives. *Appl. Microbiol. Biotechnol.* **83**, 799–808 (2009).

20. Y. Wang, S. Chen, O. Yu, Metabolic engineering of flavonoids in plants and microorganisms. *Appl. Microbiol. Biotechnol.* **91**, 949–956 (2011).

21. J. Zhou, G. Du, J. Chen, Novel fermentation processes for manufacturing plant natural products. *Curr. Opin. Biotechnol.* **25**, 17–23 (2014).

22. C. N. S. Santos, M. Koffas, G. Stephanopoulos, Optimization of a heterologous pathway for the production of flavonoids from glucose. *Metab. Eng.* **13**, 392–400 (2011).

23. D. Yang, *et al.*, Repurposing type III polyketide synthase as a malonyl-CoA biosensor for metabolic engineering in bacteria. *Proc. Natl. Acad. Sci.* **115**, 9835–9844 (2018).

24. J. Wu, T. Zhou, G. Du, J. Zhou, J. Chen, Modular optimization of heterologous pathways for de Novo synthesis of (2S)-Naringenin in *Escherichia coli*. *PLoS One* **9**, 1–9 (2014).

25. J. Wu, O. Yu, G. Du, J. Zhou, Fine-Tuning of the Fatty Acid Pathway by Synthetic Antisense RNA for Enhanced (2 S)-Naringenin Production from L-Tyrosine in *Escherichia coli*. *Appl. Environ. Microbiol.* **80**, 7283–7292 (2014).

26. J. Wu, G. Du, J. Chen, J. Zhou, Enhancing flavonoid production by systematically tuning the central metabolic pathways based on a CRISPR interference system in *Escherichia coli*. *Nat. Publ. Gr.*, 1–14 (2015).

27. S. Omura, The antibiotic cerulenin, a novel tool for biochemistry as an inhibitor of fatty acid synthesis. *Bacteriol. Rev.* **40**, 681–697 (1976).

28. Y. Lin, X. Sun, Q. Yuan, Extending shikimate pathway for the production of muconic acid. *Metab. Eng.* **23**, 62–69 (2014).

29. F. St-Pierre, *et al.*, One-Step Cloning and Chromosomal Integration of DNA. *ACS Synth. Biol.*, 537–541 (2013).

30. E. Shiu, “Improvement of D-glucaric acid production in *Escherichia coli*,” Massachusetts Institute of Technology. (2014).

31. A. Gupta, “Dynamic Regulation of Bacterial Metabolic Pathways using Autonomous, Pathway-Independent Control Strategies,” MIT. (2017).

32. L. S. Qi, *et al.*, Repurposing CRISPR as an RNA-Guided Platform for Sequence-Specific Control of Gene Expression. *Cell* **152**, 1173–1183 (2013).

557 **Figure 1.** Overview of *lux* and *esaR* quorum-sensing (QS) circuits. **(A)** Architecture of the P_{lux} (left) and P_{esaR-H} (right) QS circuits. Transcription is activated from the P_{lux} promoter when AHL-bound LuxR binds to the promoter. EsaR binds to the P_{esaR-H} promoter to block transcription, and this repression is relieved in the presence of AHL. Here, the arrow and semicircle represent the promoter and RBS, respectively. **(B)** Representative fluorescence curves showing the response of P_{lux} (left) and P_{esaR-H} (right) to varying *esaI* expression levels. Increasing *esaI* expression levels results in earlier switching from both promoters. **(C)** Representative fluorescence curves showing the response of P_{lux} (left) and P_{esaR-H} (right) to varying *luxR* expression level. Increasing *luxR* expression results in earlier switching from the P_{lux} promoter only. **(D)** Summary of the trends in switching time from the P_{lux} and P_{esaR-H} promoters varying *luxR* and *esaI* expression. Switching time was defined as the time at which fluorescence signal first surpasses a value equal to 90% of the maximum signal from the latest switcher (i.e. the lowest signal).

567

568

569 **Figure 2.** Preliminary characterization of the naringenin pathway to confirm the rationale for dual-regulation. **(A)** 570 The naringenin pathway uses four heterologous enzymes - tyrosine ammonia lyase (TAL), 4-coumaryl-CoA lyase 571 (4CL), chalcone synthase (CHS), and chalcone isomerase (CHI) - to convert L-tyrosine and malonyl-CoA to (2S)- 572 naringenin. Each mole of naringenin requires one mole of L-tyrosine and three moles of malonyl-CoA. **(B)** *p*- 573 Coumaric acid and naringenin titers with *TAL* and *4CL* expression controlled under the P_{lux} promoter. Static 574 expression of *TAL* and *4CL* at the leaky expression level (AHL (-)) or at the fully induced expression level (AHL-0 575 h) results in low naringenin titers. Exogenous induction of *TAL* and *4CL* expression during mid-exponential phase 576 (AHL 8 h) improves naringenin titers more than 6-fold; Esal-mediated induction is able to match that improvement. 577 Addition of cerulenin to increase malonyl-CoA pools results in increased naringenin titers and a decrease in *p*- 578 coumaric acid titers in all dynamic strains. **(C)** *p*-Coumaric acid and naringenin titers with *TAL* and *4CL* expression 579 controlled under the P_{esaR-H} promoter. In general, all major trends follow those observed with *TAL* and *4CL* under 580 P_{lux} control. Error bars represent s.d. of triplicate trials. *P < 0.01 compared to static controls by two-tailed *t* test. **P 581 < 0.01 compared to no cerulenin sample at same Esal level by two-tailed *t* test.

582

583

584 **Figure 3.** Dual regulation in the naringenin pathway. **(A)** Schematic of the regulatory strategy. Increasing cell 585 density triggers two dynamic gene expression switches, one that up-regulates *TAL* and *4CL* expression and a second 586 that down-regulates expression of endogenous genes that are associated with malonyl-CoA accumulation. Dotted 587 lines represent QS circuit responses and solid lines represent metabolic reaction fluxes. **(B)** Diagram of the *TAL* and 588 *4CL* upregulation module responsible for actuating the engineered response labeled (1). *TAL* and *4CL* are each under 589 their own P_{esaR-H} promoters. In the presence of constitutive EsaR and Esal, expression from the P_{esaR-H} promoter turns 590 ON with increasing cell-density. **(C)** Diagram of downregulation module responsive for actuating the engineered 591 response labeled (2). *dCas9* and each *sgRNA* are expressed from their own P_{lux} promoters. In the presence of 592 constitutive LuxR and Esal, expression of the target genes turns OFF with increasing cell density. **(D)** Naringenin 593 titers with different regulatory schemes. Naringenin titers increase 6-fold over static strategies when *TAL* and *4CL* 594 expression are induced autonomously or with the addition of exogenous AHL. Cerulenin treatment improves 595 naringenin titers in all *esaI* backgrounds and addition of the CRISPRi-mediated down-regulation module results in 596 naringenin titers that are 40% higher than the top cerulenin-treated strain. **(E)** Heat map indicating naringenin titers 597 with varying LuxR levels and down-regulation target genes. The square corresponding to the top producer is bolded. 598 *P < 0.01 compared to *TAL* and *4CL* controlled strain in L19 background. **P < 0.05 compared to *TAL* and *4CL* 599 controlled strain in L19 background with cerulenin. Error bars indicate s. d. of triplicate trials.

600

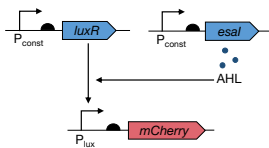
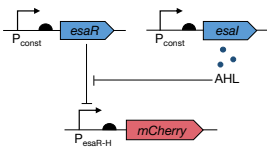
601

602

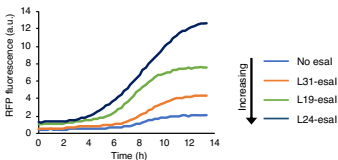
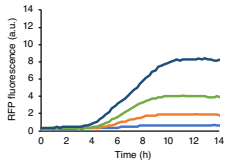
603

604 **Figure 4.** Dual-regulation in the salicylic acid pathway. **(A)** Schematic of the regulatory strategy. The genes
605 encoding the salicylic acid pathway enzymes, *entC* and *pchB*, are expressed with increasing cell-density to balance
606 growth and generation of salicylic acid, a toxic product. *pheA* and *tyrA* are silenced with increasing cell density to
607 elevate chorismate levels without introducing an auxotrophy. **(B)** Diagram of the up-regulation module. *entC* and
608 *pchB* are under control of the P_{esar-H} promoter such that increasing cell-density results in increased expression. **(C)**
609 Diagram of the down-regulation module. *dCas9* and *sgRNAs* targeted towards silencing *pheA* and *tyrA* are expressed
610 from the P_{lux} promoter. **(D)** Heat map of salicylic acid titers at varying EsaI and LuxR expression levels. Values
611 represent the mean of triplicate trials. The rectangle corresponding to the top producer is bolded. * $P < 0.01$
612 compared to constitutive *entC* and *pchB* control with no AAA pathway downregulation.

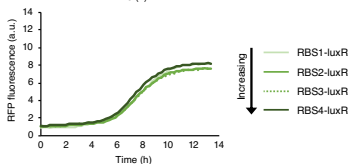
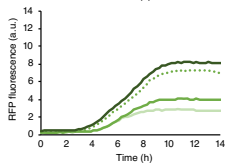
A

 P_{lux} QS Circuit **P_{esaR-H} QS Circuit**

B

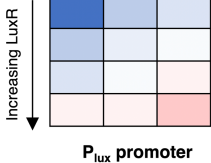


C

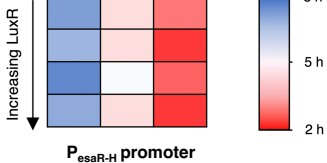


D

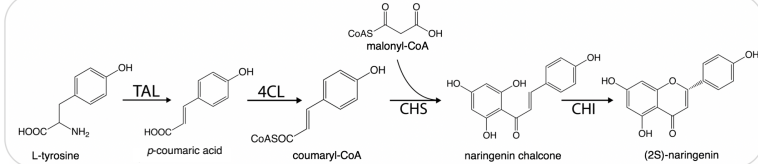
Increasing Esal

 P_{lux} promoter

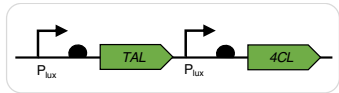
Increasing Esal

 P_{esaR-H} promoter

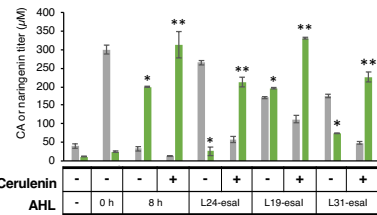
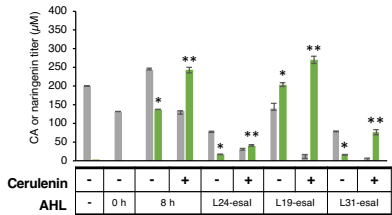
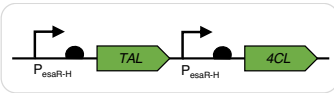
A



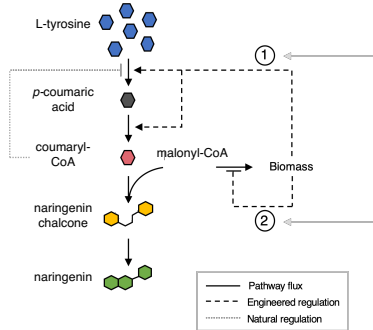
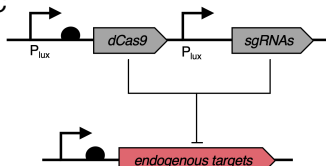
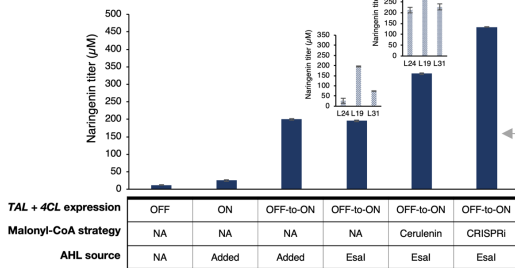
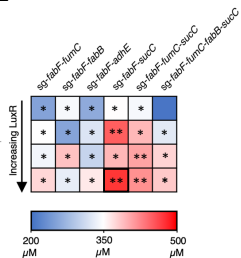
B



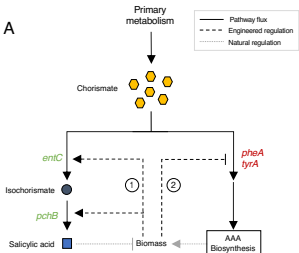
C



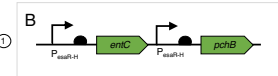
■ *p*-coumaric acid (CA) ■ naringenin

A**B****C****D****E**

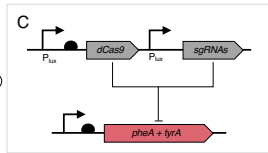
A



①



②



D

